Basin modelling workflow applied to the screening of deep aquifers for potential CO2 storage

Adriana Lemgruber-Traby, Marie-Christine Cacas, Damien Bonte, Jean-Luc Rudkiewicz, Claude Gout, Tristan Cornu

Research article

Geoenergy

https://doi.org/10.1144/geoenergy2024-010 | Vol. 2 | 2024 | geoenergy2024-010

Basin modelling workflow applied to the screening of deep aquifers for potential CO_2 storage

Adriana Lemgruber-Traby[1]*, Marie-Christine Cacas[1], Damien Bonte[1], Jean-Luc Rudkiewicz[1], Claude Gout[2,3] and Tristan Cornu[2]

[1] IFP Energies Nouvelles, 1 et 4 Av. de Bois-Préau, 92852 Rueil-Malmaison Cedex, France
[2] TotalEnergies, Pau, France
[3] Université de Pau et des Pays de l'Adour, E2S UPPA, CNRS, TotalEnergies, LFCR, Pau, France
AL-T, 0000-0002-5462-7058
*Correspondence: adriana.traby@ifpen.fr

Abstract: The temporal and spatial scale of interest of CO_2 storage studies lies in between reservoir and basin models. While reservoir modelling software is best fitted to address some of the multiphysics issues related to the behaviour of CO_2 once injected into the subsurface (adsorption, dissolution, near injection wellbore mechanics and temperature, and, in some cases, fluid rock interaction) within a human timescale, basin modelling tools handle better the full basin volume and time-scale heterogeneities that impact the storage potential and risk associated with CO_2 injection. This study takes a basin modelling approach to provide an assessment of the influence of geological evolution on CO_2 storage capacity, both at the reservoir level, by helping to estimate the amount of CO_2 that can be stored in its connected porosity, and at the cap-rock level, by assessing the seal integrity. Our basin model also captures the evolution of the pressure plume induced by the CO_2 injection, taking into account the pressure and temperature fields, aquifer connectivity and permeability, and seal integrity, on a much shorter timescale than is usually considered by such a model. The results show the impact of basin evolution on aquifer properties and consequently on the dissipation of the induced pressure plume. They also highlight the large-scale influence of the CO_2 on the pressure field both vertically along the stratigraphic column, when the pressure plume reaches shallower aquifers through unconformities, and horizontally, when good aquifer injectivity and connectivity allows the pressure plume to dissipate widely.

Thematic collection: This article is part of the Geoscience workflows for CO_2 storage collection available at: https://www.lyellcollection.org/topic/collections/geoscience-workflows-for-CO2-storage

Received 8 November 2022; **accepted** 11 April 2024

Basin modelling is one of the techniques developed to explore the subsurface and mitigate the risk in oil and gas exploration that may be adapted to the study and evaluation of the potential of large-scale deep aquifers for CO_2 storage. By integrating different data and scenarios, basin modelling simulates the deep-subsurface evolution and associated physicochemical processes that determine the present-day porosity, permeability, pressure, and temperature distribution (Doligez *et al.* 1986; Ungerer *et al.* 1990; Kauerauf and Hantschel 2009). In oil and gas exploration, basin modelling is used to simulate long-lasting, time-dependent, regional-scale phenomena such as hydrocarbon generation, migration, and entrapment, and sometimes for pore pressure prediction (Ducros *et al.* 2016; Medellin *et al.* 2018; Schneider *et al.* 2020). Some specific features of basin modelling that are essential to its original application are the large time and space scales that it encompasses, the ability to consider the variability of boundary conditions over time, and the evolutive solution of coupled equations. Each of these facets makes it possible to physically estimate, on a regional scale, properties that are sparsely sampled or only conceptually defined.

In reservoir models used to simulate and optimize hydrocarbon production, information from basin modelling simulation is rarely used. Usually, field scale geostatistical extrapolation of well data is used to characterize reservoir properties. In the case of CO_2 storage, and particularly in massive CO_2 storage in saline aquifers, much less data will be available, and it will not be economical to drill a considerable number of wells to adequately document the aquifer and seal properties (Ringrose *et al.* 2022). Furthermore, simulation of subsurface behaviour during and after CO_2 injection into saline aquifers will need to consider a larger scale than just the volume invaded by CO_2, both vertically and laterally, to properly assess lateral water migration, pressure impact and seal and fault leakage (Ringrose *et al.* 2022). Another limitation of traditional reservoir models are the isothermal assumptions usually made, despite the temperature dependency of CO_2 properties and phase behaviour (Ringrose *et al.* 2022).

The use of basin models focused on the evolution of petrophysical properties, estimation of fluid content, and pressure and temperature fields and can thus be of great use to define and constrain CO_2 injection models. In basin models, regional data and different conceptual geological scenarios can be integrated into the simulations. The effect of past processes affecting present day properties, such as erosion, diagenesis, and natural fracturation, can be taken into account in these models. New developments underway, focusing on the application of basin models to the screening of CO_2 storage areas, allow the simulation of the dissipation of the pressure plume generated by the massive fluid injection on aquifers. A real sedimentary basin case is used to demonstrate the added value of a new workflow supported by an enhanced basin model simulator. Other developments and workflows under investigation will be discussed.

Techniques, workflow and experimental set-up

Basin modelling

First developments of basin modelling tools started in the 1980s with the coupling of backstripping and forward simulations to assess the hydrocarbon generation and migration history (Steckler

et al. 1988; Ungerer *et al.* 1990; Hantschel and Wygrala 2019). Since then, the complexity of basin models has increased, making it possible to integrate different coupled processes and to simulate higher resolution 3D models and unstructured meshes (Guichet *et al.* 2009; Faille *et al.* 2014; Gonzalez-Penagos *et al.* 2015; Bruch *et al.* 2021; Torelli *et al.* 2021).

Basin modelling starts with the construction of a present-day geomodel that integrates structural, stratigraphic, sedimentologic and petrophysics data, that defines the geometry of the different layers, associated depositional age, and facies distribution in each layer. In the traditional use of basin modelling, the definition of the source rock intervals and their organic characteristics are also needed, but this is irrelevant to this work. The model description of a basin's heterogeneity is limited by the model resolution and the input data. Relatively homogeneous models can be defined using regional palaeoenvironment maps for the different layers, while forward stratigraphic models can be used to increase the resolution of the facies variations and provide a way to generate different facies distribution scenarios (Granjeon 1997; Arab *et al.* 2016). Higher resolution facies heterogeneity can also be defined using seismic attributes (Lemgruber *et al.* 2010). Each facies is associated with a set of constitutive laws that includes compaction curves, porosity-permeability relationship, and thermal properties (Ungerer *et al.* 1990).

Once the present-day model is defined, the past model geometry is calculated, considering pre-defined palaeo-bathymetries, erosion events, and associated eroded thicknesses using backstripping or structural restoration techniques (Perrier and Quiblier 1974; Steckler and Watts 1978). At this step, porosity-depth curves are used to calculate the evolution of layer thickness through time. The coupled thermo-hydro-mechanical forward simulation is computed from the resulting model geometry evolution. In the present study, the fluid flow is simulated using a Darcy law coupled with the compaction law and taking into account regional pressure gradients. Permeabilities are calculated according to the porosity-permeability relation assigned for each lithology (Ungerer *et al.* 1990). The effect of sediments loading on porosity does not depend only on the burial but also on the overpressure and associated low effective stress (Schneider *et al.* 1993), which may be generated during high sedimentation periods associated with low permeability, leading to undercompaction of sediments (Mello and Karner 1996). The temperature calculation is performed using a heat conservation equation that takes into account conductive and advective heat transfer, radiogenic heat generation, surface palaeotemperature, and basal heat flow (Enchéry 2004). The model thermal properties (i.e. conductivity, mass heat capacity and radiogenic production) vary and evolve according to the defined facies and calculated temperature and porosity, taking also into account the properties defined for the pore filling brine (Enchéry 2004).

A set of properties results from this geological basin modelling at each time step of the basin evolution (Fig. 1). These properties include (but are not limited to) porosity, permeability, brine pressure, geostatic stress, effective stress, and temperature. The model is validated by comparing the resulting properties with the available surface and well data (present-day borehole and surface temperature, heat-flow, borehole formation pressure, palaeo-indicators such as vitrinite reflectance measurements), after adjusting facies and/or brine properties and constitutive laws, boundary conditions, and defined hypotheses (such as erosional events) during a trial-and-error calibration process.

Experimental workflow: from geological to forecast basin model

The geological basin model results can be used for a first identification and selection of areas most suitable for the CO_2 injection, in terms of available connected porous space and best injectivity. They can also be used to initialize reservoir model properties (pressure, temperature, porosity and permeability) or to provide lateral boundary conditions of e.g. pressure to reservoir models, although significant downscaling work may be required to transfer data between simulators. Recent developments on the basin model Arctem® calculator (Faille *et al.* 2014) make it possible to design a new workflow: the simulated present-day properties are used as initial conditions for the injection of fluid in selected cells of the basin model to follow the dissipation of the pressure plume created by the fluid injection, using an adapted time step computation (Fig. 1). These developments of a forecast basin model aim to provide a first order assessment of the extent of the pressure plume and of the resulting pressure increase far from the injection point considering aquifer connectivity, seal integrity and, in some cases, fault properties. The additional inputs required for this step are the duration, location, and volume of the injected fluid. In the same basin model, the duration of the simulated events considered during the injection and post-injection phases (10s of years) are considerably smaller than those used during the geological evolution of the basin (1–10s of millions of years). In both cases, the minimum calculation time step handled by the Arctem calculator is 0.1 years (~36 days), which was sufficient to achieve calculation convergence in the present study. . The results analysis was performed using post-processing calculators for the geological basin model and forecast basin model analysis. The experimentation of this workflow with a real dataset on a sedimentary basin aimed at providing a simple application example to illustrate the importance of considering coupled multiphysics simulations at the basin scale to highlight the impact of basin history on present-day properties.

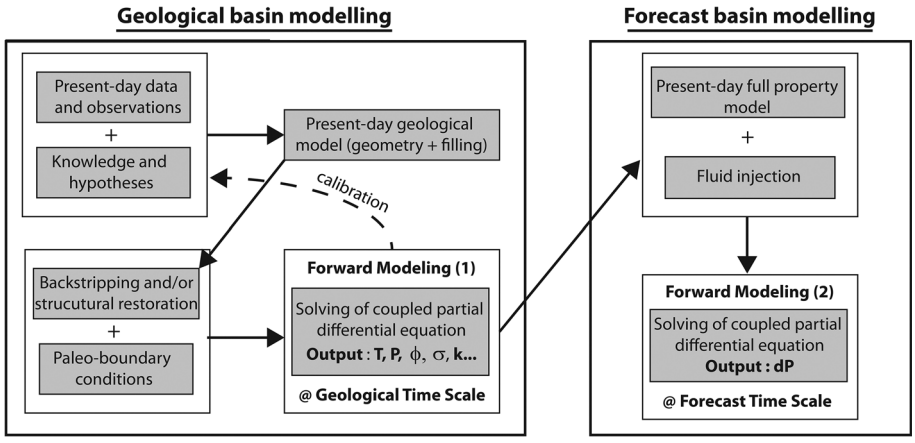

Fig. 1. Basin modelling workflow extended and applied to the screening of potential CO_2 storage areas, including simulation of the geological basin history with traditional Geological basin modelling workflow and the simulation the CO_2 injection effect at shorter time scale with Forecast basin modelling workflow.

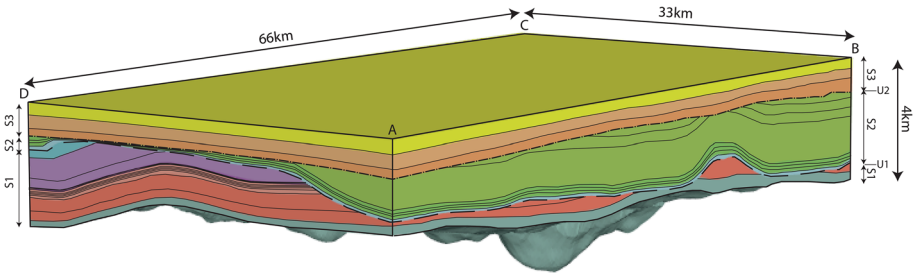

Fig. 2. 3D basin model. In order to anonymize the model position, its orientation is given by letters A, B, C and D. Colours correspond to different stratigraphic units; lines correspond to layer boundaries. S1, S2, S3 correspond to the different sequences separated by unconformities U1 and U2.

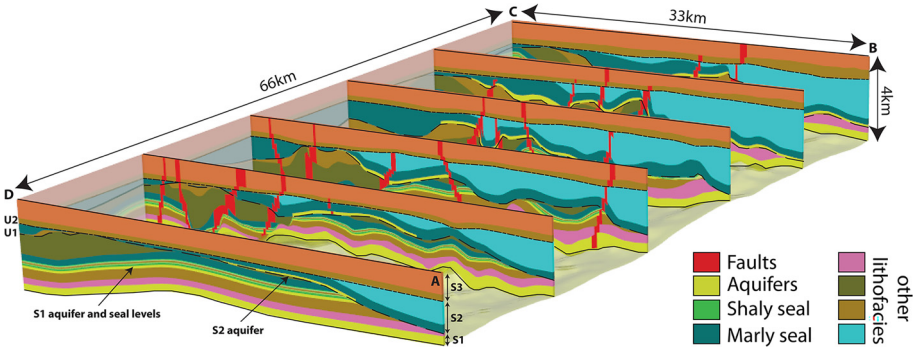

Fig. 3. 3D shaded block and superimposed fence diagram showing the facies distribution defined for the basin model and the location of aquifers.

Geological basin model experimental case

An application example of the use of this new workflow was performed to demonstrate the capabilities of enhanced basin model simulation for the screening of storage of CO_2 in deep aquifers. The modelled basin is based on a natural case that is anonymised due to confidentiality issues. It consists of a 66 km long and 33 km wide 3D basin model ranging in thickness from 1.95 to 7.5 km with 28 layers in 3 sequences bounded by 2 unconformities (Fig. 2). Depth-structure maps obtained from seismic interpretation were used to define the geometry of the main units. Additional subdivisions were included in the model to account for vertical heterogeneity, based on litho-stratigraphic data from wells. These additional subdivisions allow us to better individualize the main aquifer and seal levels (Fig. 2). The lateral resolution of the cells is 250 m, which is the resolution of the regional maps, and the vertical resolution, that corresponds to the layer to the layers thickness, varies from 0 m to 1.2 km.

Potentially interesting aquifer reservoir levels are present at the middle of sequence S1 and at the base of sequence S2 (Fig. 3). The S1 aquifers consist of three stacked aquifer-seal pairs, whereas only one aquifer interval is present at the bottom of sequence S2, just above the unconformity U1 that separates sequences S1 and S2. The facies distribution in the model was defined according to regional palaeo environment maps that are mainly homogeneous in the model area, except for the S2 aquifer, which has good aquifer characteristics (sandy facies) only locally and is shaly elsewhere (Fig. 4).

Compaction curves and porosity-permeability curves from data locally available for all reservoir aquifer levels were used for the modelled aquifer facies. For the other facies, the default parameters available from the software lithological library were selected in accordance with the palaeoenvironment and lithological content. Several faults were mapped at the study area. Since the basin modelling was performed on a structured grid, these faults were represented as specific facies (Figs 3, 4). It was chosen to model these faults as flow barriers ($k < 0.02$ mD). Likewise, no vertical flux was simulated along these faults.

Two erosion events associated with the unconformities were taken into account. The first erosion event affected sequence S1 and locally eroded the S1 aquifer and seal levels (Figs 3, 4). The second erosion event took place after the deposition of sequence S2. The aquifer and seal levels of sequence S1 were uplifted but not further eroded by this second erosion (Fig. 5). The reference geological model scenario was defined according to the results of previous studies where the amount of eroded thickness was obtained from the calibration with vitrinite reflectance data. This reference erosion scenario allowed us to simulate the model burial evolution and its effect on present day properties. Because eroded thickness is a major uncertainty, two alternative scenarios were modelled. One considering there is no erosion, in which the maximum burial is the present-day burial, and another one considering a more intense erosion (Fig. 6). In this last scenario, the amount of eroded thickness was calculated by considering that the eroded layers were isopachous during deposition. For that, the maximum thickness of the layer, backstripped to its deposition time, was considered and the

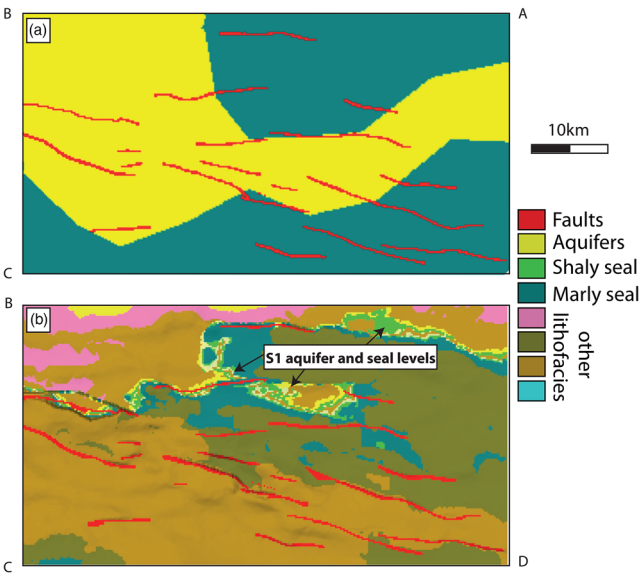

Fig. 4. (**a**) Facies map of base of sequence S2; (**b**) subcrop map at U1 unconformity showing remaining S1 units. Colours correspond to facies as described in the legend.

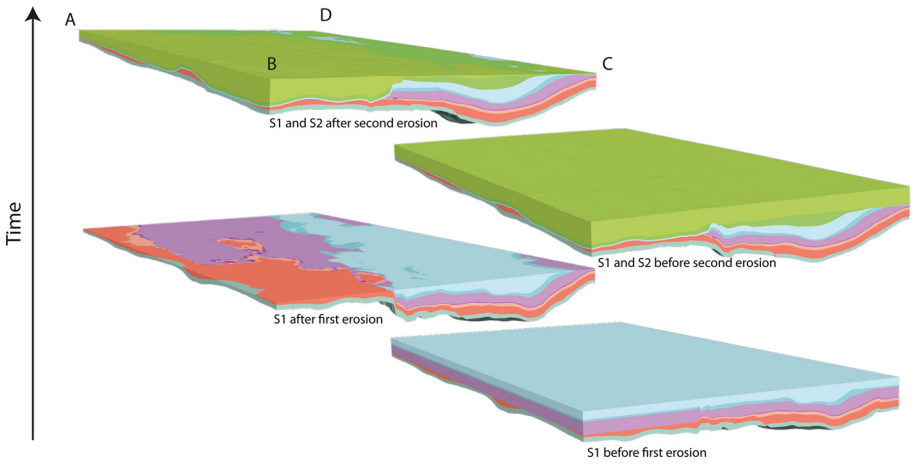

Fig. 5. Geological basin model evolution at four steps for the reference scenario. From bottom to top: first block corresponds to basin geometry, at end of sequence S1 deposition, before first erosion. Second block corresponds to model geometry after first erosion. Third block corresponds to basin geometry, including sequences S1 and S2, before the second erosion. Upper block corresponds to model geometry after second erosion. Colours correspond to model stratigraphy as presented in Figure 2.

eroded thickness was calculated by subtracting the remaining thickness map from the calculated maximum thickness.

Finally, the thermal boundary conditions were defined. The basal palaeo-heat flow was prescribed according to previous regional studies that took into account basin evolution and calibration with thermal data, and the palaeo-surface temperature was set considering the palaeo-latitude and associated climate as well as the palaeo-bathymetry. No flow was considered outside of the model lateral and bottom boundaries.

Results of the geological basin model

The basin modelling results were compared with the available well data for the model calibration. The pore-filling brine salinity and corresponding density were defined according to the available data in order to correctly reproduce the hydrostatic pressure trend observed on wells (Fig. 7). The locally sub-hydrostatic pore pressure and low porosities measured at wells were also reproduced by the geological basin model. Modelling the burial history evolution allowed us to reproduce part of the wide range of porosities that are observed at a same present-day burial depth for a given lithology (Fig. 8). But additional porosity heterogeneity known to be the result of diagenetic processes was not addressed in this work.

As expected, varying the amount of eroded thickness strongly affected both the porosity and the porosity- and facies-dependent permeability results (Fig. 9).Without taking into account the erosion events and resulting maximum past burial, the permeabilities obtained for the deep aquifer layers are up to 10 times higher than in the reference scenario. In contrary, when increasing the amount of eroded thickness, the permeability results are up to five times lower than in the reference scenario. The variation of the porosity results according to erosion scenario is up to 20%, higher in the scenario without modelled erosion, and lower in the scenario with higher amount of eroded thickness.

Static screening of CO_2 storage areas with geological basin model

The geological basin modelling results were used to calculate key parameters that allowed a quick look analysis and selection of best areas for the CO_2 injection at the target aquifers located at sequence S1. First, a capacity index map corresponding to the porous volume per cell area was calculated to account for the space available for containing fluid. A simplistic injectivity index map per aquifer cell was obtained by multiplying the permeability by the layer thickness. Finally, a potential index map was obtained by multiplying the capacity and injectivity indexes of the three stacked reservoirs of sequence S1 (Fig. 10). This static potential calculated for the target aquifers shows a high heterogeneity, as observed for the permeability and porosity results. This map was used for the

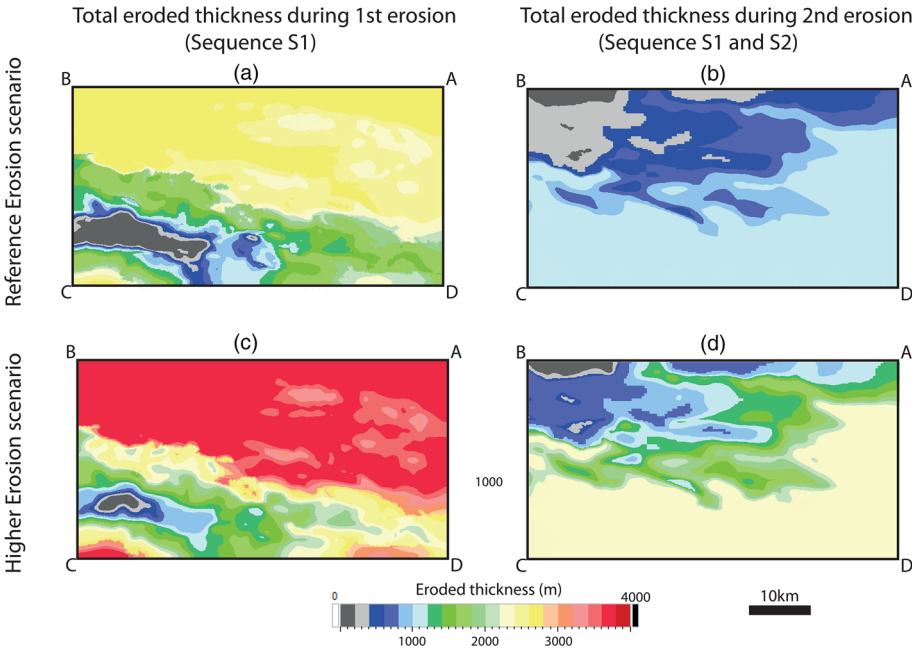

Fig. 6. Eroded thickness maps used in reference and higher erosion scenarios. The presented thicknesses correspond to the total thickness removed by each erosion event on the stack of layers.

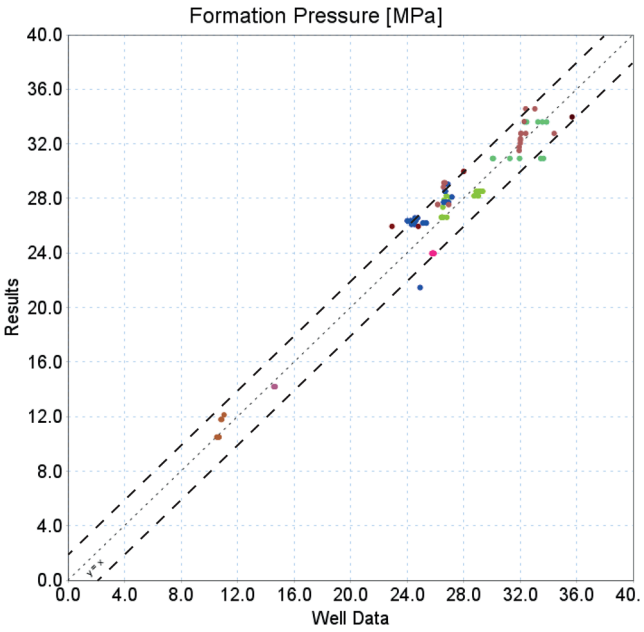

Fig. 7. Pressure calibration cross plot. Horizontal axis corresponds to well data formation pressure measurements and the vertical axis corresponds to the model results at the same location. The dotted line corresponds to $X = Y$, and the dashed lines correspond to ±10% tolerance. Colours refer to different wells.

selection of the injection point for the dynamic simulation with the forecast basin model (Fig. 10).

Forecast basin model experimental case

In our experiment, the deeper aquifers, present in sequence S1, were selected as the target aquifers for the CO_2 injection due to their deeper location, continuity, and regional seal. The fluid injection was located at an optimized site, defined from a screening of the simulated geological basin model by considering the connected pore volume reachable by an injection well, aquifer depth and number of aquifers (Fig. 10). The forecast basin model experiment simulated the pressure plume development and dissipation following the fluid injection, considering only single-phase flow. It simulated the pressure wave generated by the fluid injection, but not the dissipation of the fluid itself, nor did it consider CO_2 dissolution and fluid–rock interactions, that may induce fluid volume variation as a function of pressure and temperature variation through time.

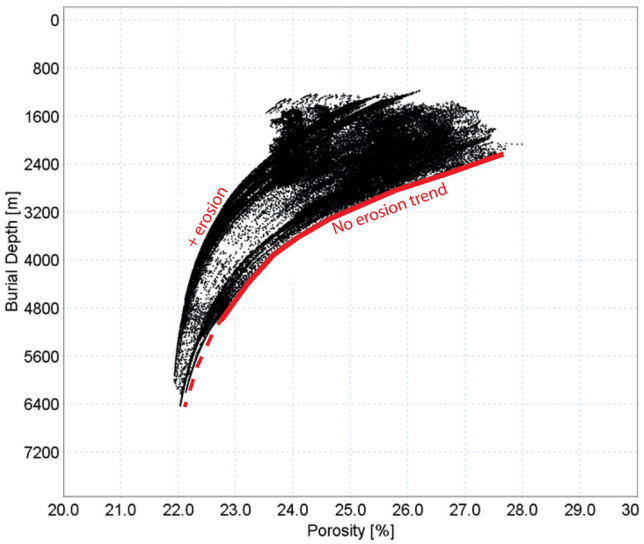

Fig. 8. Geological basin model results: porosity v. present-day burial depth cross plot for target aquifers (S1) lithofacies. Each point represents the basin model results at one cell of the reference erosion scenario model. The no erosion trend corresponds to the cells located in areas not affected by the erosion episodes.

In the designed reference case scenario, the prescribed injection rate was of 2×10^6 m^3/year, which corresponds to 1 $MtCO_2$/year if a density of about 500 kg m^{-3} is considered. This is a similar rate to injection rates actually achieved in real projects (Chadwick *et al.* 2008; Michael *et al.* 2010; Celia *et al.* 2015). For example, at In Salah, the CO_2 injection rate was about 1 Mt/year (Haddadji 2006), and at Spleiner, the injection rate started as 0.9 Mt/year, and was slightly decreased since then (Furre *et al.* 2017, 2024). In our forecast model, the total injection rate was distributed in the three deep aquifers of S1. The injection persisted for 20 years, and the pressure plume dissipation was simulated for 30 years after the end of the injection. Alternative injection scenarios were designed to investigate both the influence of the permeability parameters related to the basin modelling erosion scenarios results and the fluid injection flow rate (Table 1). The number of wells was raised to 4 for the high injection rate scenarios, within 3 km of the initial target location.

Forecast basin model dynamic results

The pressure increase resulting from the fluid injection was calculated in the entire model by the difference between the pressure computed after the injection period and the formation pressure prior to the fluid injection, which corresponds to the pressure resulting from the geological basin model simulation. This pressure increase was calculated both immediately after the fluid injection and 30 years after the end of the injection. The results show that the influence of the injection on the pressure regime is observed up to the boundaries of the model, 40 km from the injection and that the pressure increase reaches the shallow aquifer of sequence S2 (Fig. 11). Although the stronger pressure increase occurs during the injection, with a maximum pressure increase in excess of 2 MPa, it starts dissipating and is still equilibrating 30 years after the end of the injection. Updip from the injection point the pressure build-up keeps increasing 30 years after the end of the injection. The increase in absolute pressure in these shallower areas is up to 0.5 MPa, which is lower than the one observed close to injection point, but may have a higher impact on the seal stability due to its lower consolidation. This increase in pressure far away from the injection point could also affect fault stability.

The geological basin modelling simulation calculates the geostatic pressure that can be related to the vertical stress, but it does not estimate nor handle horizontal stresses. Recent work made it possible to integrate a geomechanical calculation and regional tectonics into the basin modelling simulation (Berthelon *et al.* 2021), but these developments are not yet appliable to the fluid injection simulations. In this paper, for an initial assessment of the risk of fracturing, we assume that fracturing follows a tensile vertical failure criterion (Schneider *et al.* 1999) with the conservative hypothesis that the tensile strength of the rock is negligible with respect to the stress level at great depth. It follows that fracturing can occur when $P > \sigma_h$ i.e. when $(P/\sigma_v) > K_0$, where P is the formation pressure, σ_v and σ_h are the vertical and minimum horizontal total stresses and K_0 is the ratio σ_h/σ_v. A fracture index K and a fracture threshold FT are introduced and defined as follows:

$$K = \frac{P}{\sigma_v} \tag{1}$$

$$FT = \frac{P}{K_0 * \sigma_v} \tag{2}$$

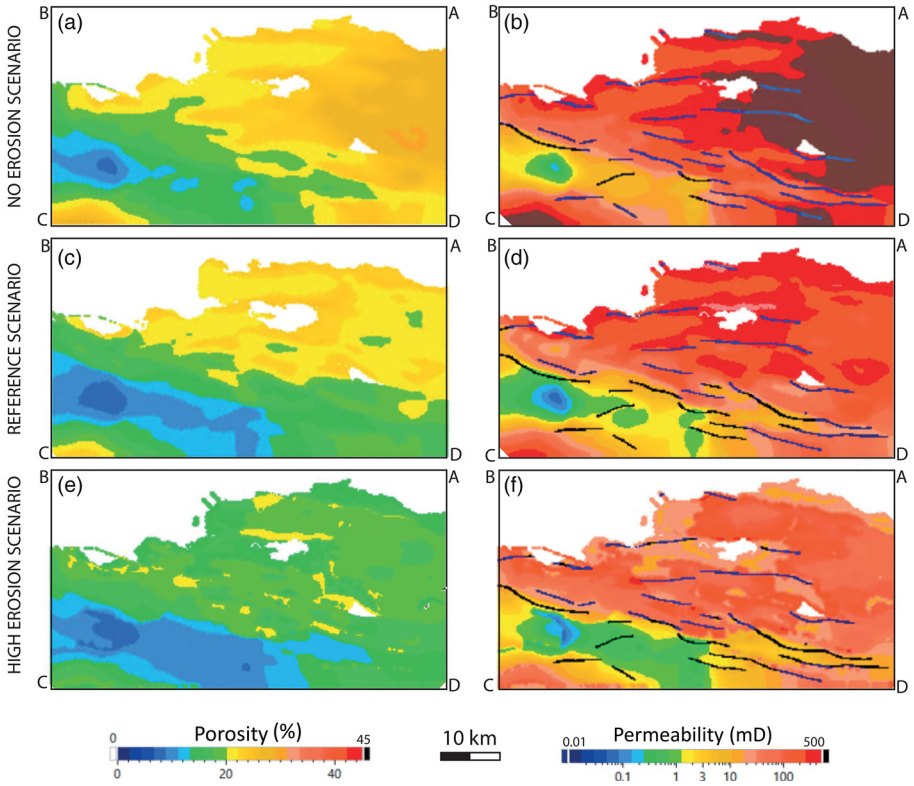

Fig. 9. Geological basin model results: porosity (left) and permeability (right) computed for the deepest target aquifer of sequence S1. The central maps correspond to the results of the reference scenario; the uppermost maps correspond to the results of the no erosion scenario and the lowermost maps correspond to the maximum erosion scenario considering isopach layer deposition for the eroded layers. Blue cells on permeability maps correspond to fault facies with near-zero permeability.

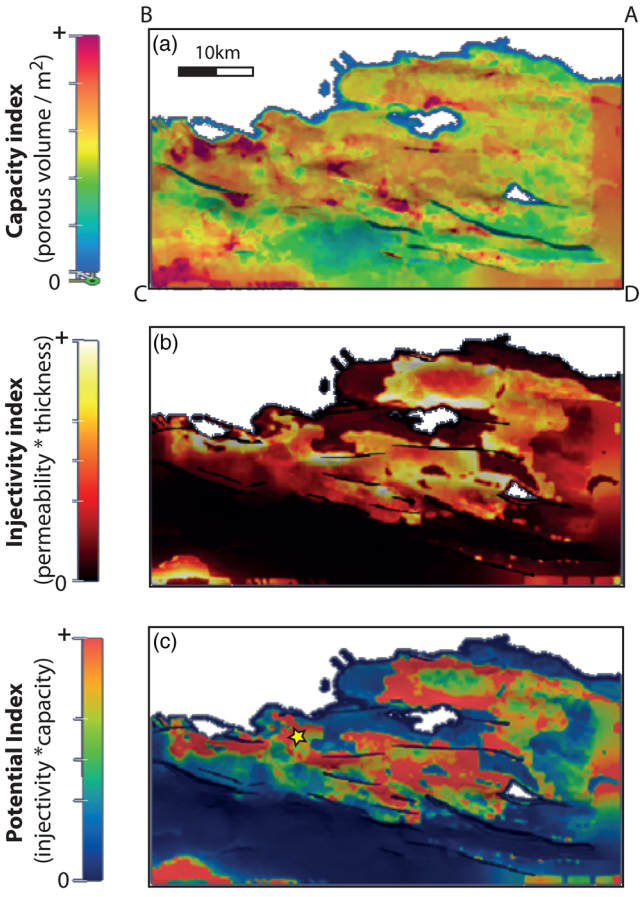

Fig. 10. CO_2 injection static potential calculated for the deepest target aquifer of sequence S1. The maps show the capacity, injectivity and potential index maps calculated using the layer thickness and the porosity and permeability results obtained from geological basin modelling for the reference erosion scenario. The yellow star indicates the selected location for the fluid injection reference case Sc1.

where K is the stress ratio, K_0 is the critical stress ratio, defined with a fixed value of 0.6, and FT is the fracture threshold. Fracturing can occur in areas where K is higher than the *in situ* stress ratio K_0, or where FT $>$ 1, assuming the *in situ* stress ratio is uniform and equal to K_0.

The reference case (Sc 1) results show that the higher fracture threshold observed at the target aquifer are lower than 0.95 (Fig. 12a), indicating that regionally the risk of damaging the seal integrity (fracture threshold >1) is negligible with the reference injection scenario. In all injection scenarios (Table 1) the pressure plume reaches the upper aquifer by crossing the S2 unconformity. In contrast to the reference case, the fracture threshold FT is reached for the seal layer above the target aquifer in all alternative scenarios (Fig. 12). When increasing the volume of fluid injected and reducing the aquifer permeability (Scenario Sc2, Fig. 12b), the pressure plume effect remains close to the injection point and fracture threshold above 1 is restrained to a small area. In the scenarios considering a higher fluid injection rate from 4 (four) wells, using the reference case permeability (Scenario Sc3, Fig. 12c) or considering higher permeability for the S1 aquifers (Scenario Sc4, Fig. 12d), the defined fracture threshold is reached in a wider area than for Scenario

Table 1. Injection scenarios defined and simulated with forecast basin modelling

Scenario	Aquifer permeability	Injection flow rate (Mt y^{-1})	Number of wells
Reference case (Sc1)	reference geological basin model permeability	1	1
Scenario 2 (Sc2)	ref/5 (higher erosion sc. permeability)	2.5	1
Scenario 3 (Sc3)	reference geological basin model permeability	6	4
Scenario 4 (Sc4)	ref*10 (no erosion sc. permeability)	6	4

Erosion scenarios refer to geological basin models scenarios that impact the aquifer permeability. Injection flow rate impact the number of injection wells.

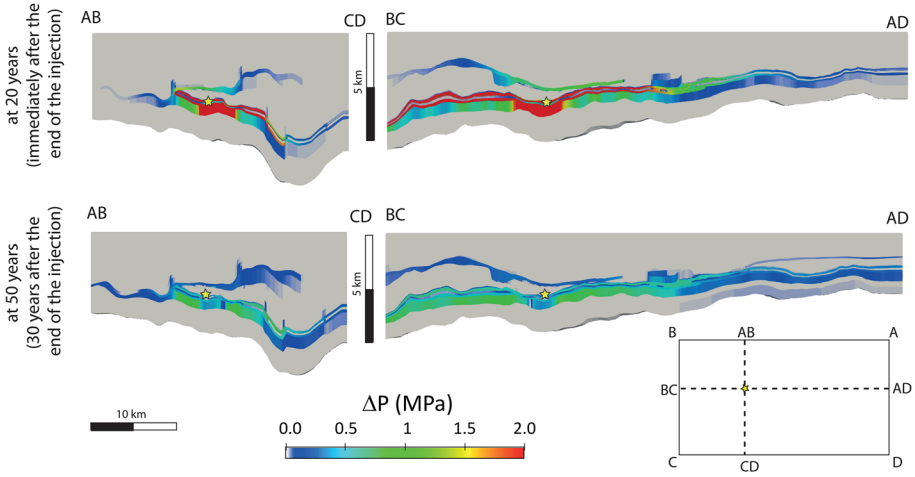

Fig. 11. Pressure evolution along 2 (two) cross sections in the forecast basin model reference scenario Sc1. The fluid injection point is the yellow star, located at the intersection of the cross sections. The uppermost sections present the pressure increase at the end of the 20 years injection; the lowermost sections present the remaining pressure increase 30 years after the end of fluid injection.

Sc2. In scenario Sc3, although the pressure plume dissipates quite widely, the areas where the fracture threshold is reached are located around the injection point. In scenario Sc4, the high permeability of the aquifer, allows a highly efficient pressure dissipation, preventing the pressure increase close to the injection point. Instead, the pressure rise is transferred laterally towards zones with lower vertical stress, and the defined fracture threshold is reached far away from the injection point (Fig. 12d). In these areas, the vertical stress is small, and a small increase of the formation pressure corresponds to a significant increase towards the fracture threshold.

Discussion

The presented work aimed at illustrating two aspects of basin modelling that allow both a fast-track semi-quantitative assessment of deep aquifers for CO_2 storage and the location of injection areas. First, we have shown that geological basin modelling can calculate present day properties by integrating scarce present-day information, geological scenarios, and the physical processes prevailing during basin evolution. Secondly, we have shown that basin models can also be used as large-scale forecast basin models to test the impact of massive fluid injection on the overall behaviour of a basin system, comprising inter-connected aquifers, drains, and seals, highlighting risks of leakage. The workflow developed allows (1) the building of a large scale geological model that can be constructed from regional structural maps and regional facies distribution maps, in a sedimentary basin, (2) the mutliphysics simulation of the geological history of the basin, providing the property evolution and distribution in the model from deposition to present day, (3) the calibration of the geological basin model to sparse well static data (porosity, permeability, fluid content) and dynamic (pressure, temperature), (4) the analysis of this model to identify relevant connected pore volumes as large scale aquifers and identification of favourable injection areas, (5) the simulation of fluid injection scenarios in the same gridded model and (6) the analysis of the resulting forecast basin models to qualitatively assess aquifer seal integrity on selected injection scenarios. The impact of the erosion and uplift on the porosity and permeability of aquifers was analysed using simplified relations and can be used only qualitatively. Additional heterogeneity, such as facies distribution, or processes, such as diagenesis, could be also added to the geological basin model in order to test their influence and the impact of their associated uncertainty on the CO_2 storage potential and associated risk.

Starting from the same model, injection simulations with a far smaller time step show that the pressure wave has a far-field impact on overpressure and on seal integrity. This is the case when the reservoirs are interconnected and the geometric gradients are strong.

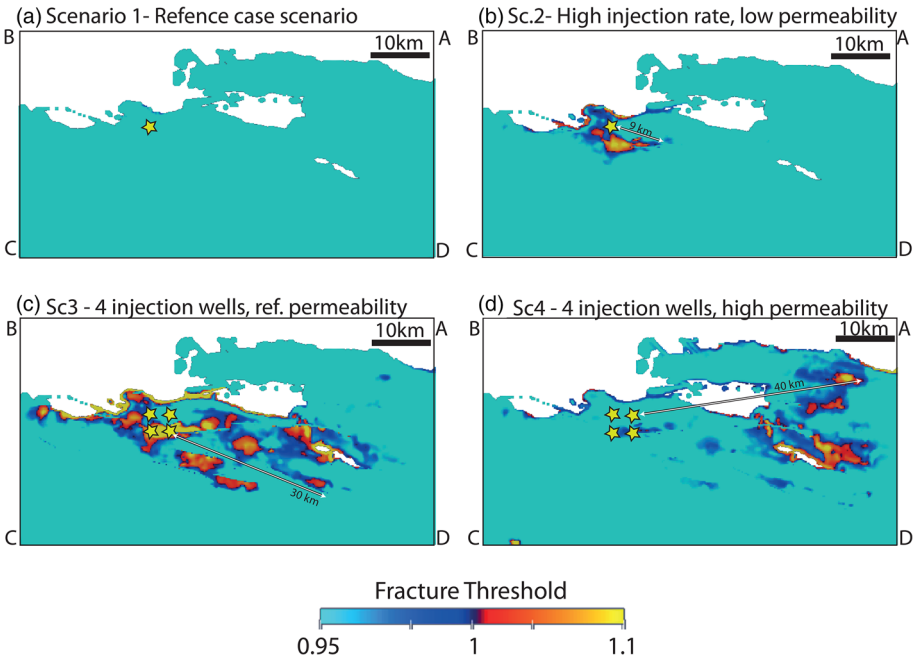

Fig. 12. Fracture threshold calculated at the end of the 20 years injection for the different injection scenarios (Table 1), using the formation pressure and geostatic stress results and a defined critical stress ration of 0.6 (equation 2). The maps correspond to the cap-rock layer located above the target aquifer (upper S1 aquifer). The yellow stars indicate the fluid injection locations for the different scenarios.

The modelling of far-field impact on overpressure may be crucial to the analysis of fault and seal integrity, since the weak and critical areas may be located far from the injection point, for example at areas with lower consolidation or at near-critical stress faults. The impact of the fluid injection on the aquifer seal integrity was analysed using simplified relations and can be used only qualitatively. Additional work is necessary to properly investigate the potential brittle failure of the seal rocks by coupling the basin-scale fluid injection simulation to a geomechanical model. This coupling between geological basin modelling and geomechanical simulation has already been successfully applied to predict natural fracturing (Berthelon *et al.* 2021; Bruch *et al.* 2021), but additional research work is necessary to apply it to the calculation of the geomechanical response to fluid injection simulations. The experiment did not consider any flow along faults or fractured seals, potentially damaged due to pressure wave impact, but additional work could consider the modification of the hydraulic permeability of seal and fault-facies once the fracture threshold is reached, impacting the pressure redistribution. Fault representation could be improved: recent developments on unstructured grids allows explicit representation of faults and their associated fluid flow in basin models (Faille *et al.* 2014; Woillez *et al.* 2017). With this technology, unstructured basin modelling with explicitly-represented faults can be used to simulate the fluid injection and its results can be used as initial conditions for reservoir models. However, challenges remain to simulate certain configurations in 3D unstructured meshes, such as fault crossing and unconformities. Ongoing developments are tackling this issue (Li *et al.* 2021). The presented workflow and tools could in the future be applied to unstructured meshes and coupled to geomechanical modelling to investigate fault stability during pressure and fluid dissipation.

In the presented work, little attention was given to the thermal conditions, both their evolution and present-day conditions. This is justified by the choice to focus on modelling single-phase pressure dissipation and the impact of subsidence and erosion history on present-day rock properties. The workflow could be improved by integrating diagenetic processes and their impact on the petrophysical properties (Schneider *et al.* 2003). In this case, the impact of temperature evolution would need to be better constrained to account for the kinetics of the diagenetic processes. Current work on the integration of fluid chemistry during basin evolution could also give useful information concerning past fluid–rock interactions and their impact on present day petrophysical properties. Since present-day temperatures affect the physical state of CO_2, the temperature conditions would also play a key role when considering a two-phase fluid flow.

Important simplifications were made during the forecast basin modelling simulations, by neglecting changes in CO_2 volume, phase and properties, and fluid–rock interactions. These processes are well accounted for in reservoir modelling and usually analysed in detail in smaller-scale models. Defining proper boundary conditions may be challenging in these models. Results from geological basin modelling, such as porosity, permeability, pressure and temperature fields, can be used to define the initial conditions (i.e. initialize) reservoir models. An interesting evolution of the presented workflow could also be to couple the results of forecast basin models to constrain the evolution of boundary conditions during CO_2 injection in a reservoir model.

Conclusion

With the present work we show that a sparsely-constrained, process-based large-scale geological basin model simulation can deliver first order insights on porosity, seal quality distribution, aquifers connectivity through unconformities, faults or uncomplete seal layers. It makes it possible to estimate the regional present-day petrophysical properties, as well as pressure and temperature fields by simulating the geological basin evolution. These properties were used for static screening of best location for CO_2 injection, and as initial conditions for the fast-track dynamic simulations of pressure dissipation related to fluid injections in a forecast basin model.

Once the reference geological basin model is created, different alternative scenarios can be simulated to understand the model uncertainty and to calculate realistic alternative initial scenarios for the simulation of CO_2 injection at specific locations. By using the basin model as a forecast tool, the presented workflow makes it possible to have a first idea on the mechanisms and pathways of pressure dissipation, at a regional scale, during and after fluid injection with variable injection rates and locations. This can help to identify key properties or areas that seem to have a higher impact on the seal integrity and that need to be better constrained to limit the risk associated with the CO_2 storage in basin scale aquifers.

By addressing the impact of burial evolution scenarios, the presented application example illustrates that the prediction of lateral variations of capacity and injectivity is not only controlled by present-day depth and lithology. The geological basin model scenario results demonstrated the impact of geological history on present day properties, and the results of the forecast basin model scenarios considering different permeabilities demonstrated the impact of geological history on the pressure plume extent and dissipation. The fluid injection simulations considered total injected volumes ranging from 20 to 120 Mt of CO_2 and showed that the leakage and fracturing risks are limited. However, they also showed that the pressure increase induced by fluid injection reached the model's borders, 40 km from the injection point, highlighting the importance of taking into account the regional scale to include the entire plumbing system. They highlighted the possible connection between the two aquifers through an unconformity, and that the weak points of the system may be located far from the injection point at an updip position of the aquifer.

Several possibilities of improvement of this workflow can be suggested that need additional developments. These improvements include (1) the coupling of geomechanical simulation to the forecast basin modelling, (2) considering fluid redistribution due to changes of seal integrity, (3) using unstructured grids to better simulate faults geometry and properties, and (4) linking basin modelling results to CO_2 injection simulation in reservoir modelling tools. With regards to the latter, the results of geological basin modelling could be used to initialize reservoir model properties, and the results of large-scale forecast basin modelling could be used to prescribe the evolution of the boundary conditions of dedicated reservoir modelling during CO_2 injection simulations.

Acknowledgements We would also like to thank Lorcan Kennan and an anonymous reviewer for the valuable comments and suggestions that helped improve the quality of the manuscript.

Author contributions **AL-T**: conceptualization (equal), investigation (equal), methodology (equal), validation (equal), writing – original draft (lead), writing – review & editing (equal); **M-CC**: conceptualization (equal), investigation (equal), methodology (equal), project administration (equal), supervision (lead), validation (equal), writing – review & editing (equal); **DB**: conceptualization (lead); **J-LR**: supervision (equal), writing – review & editing (equal); **CG**: conceptualization (equal), project administration (equal), supervision (lead), writing – review & editing (equal); **TC**: project administration (equal), supervision (equal)

Funding The authors acknowledge TotalEnergies and IFP Energies Nouvelles for funding this project.

Competing interests The authors declare that they have no known competing financial interests or personal relationships that could have appeared to influence the work reported in this paper.

Data availability Data sharing is not applicable to this article as it concerns the workflow and not a specific dataset.

References

Arab, M., Belhai, D. *et al.* 2016. Coupling stratigraphic and petroleum system modelling tools in complex tectonic domains: case study in the North Algerian Offshore. *Arabian Journal of Geosciences*, **9**, 289, https://doi.org/10.1007/s12517-015-2296-3

Berthelon, J., Brüch, A. *et al.* 2021. Impact of tectonic shortening on fluid overpressure in petroleum system modelling: insights from the Neuquén basin, Argentina. *Marine and Petroleum Geology*, **127**, 104933, https://doi.org/10.1016/j.marpetgeo.2021.104933

Bruch, A., Colombo, C., Frey, J., Berthelon, J., Cacas-Stentz, M.C., Cornu, T. and Gout, C. 2021. Coupling 3D geomechanics to classical sedimentary basin modelling: from gravitational compaction to tectonics. *Geomechanics for Energy and the Environment*, **28**, 100259, https://doi.org/10.1016/j.gete.2021.100259

Celia, M.A., Bachu, S., Nordbotten, J.M. and Bandilla, K.W. 2015. Status of CO_2 storage in deep saline aquifers with emphasis on modeling approaches and practical simulations. *Water Resources Research*, **51**, 6846–6892, https://doi.org/10.1002/2015WR017609

Chadwick, R., Arts, R., Bernstone, C., May, F., Thibeau, S. and Zweigel, P. 2008. *Best Practice for the Storage of CO2 in Saline Aquifers*. *British Geological Survey Occasional Publication*, **14**. Keyworth, Nottingham.

Doligez, B., Bessis, F., Burrus, J., Ungerer, P. and Chenet, P.Y. 1986. Integrated numerical simulation of sedimentation, heat transfer, hydrocarbon formation and fluid migration in a sedimentary basin: the Themis Model. Thermal Modelling in Sedimentary Basins, Proceedings of the 1st IFP Research Conference on Exploration, 3–7 June 1985, Carcans, 173–195.

Ducros, M., Carpentier, B., Wolf, S. and Cacas, M.C. 2016. Integration of biodegradation and migration of petroleum in a 2D petroleum system model: application to potiguar basin, NE Brazil. *Journal of Petroleum Geology*, **39**, 61–78, https://doi.org/10.1111/jpg.12628

Enchéry, G. 2004. *Modèles et schémas numériques pour la simulation de genèse de bassins sédimentaires*. PhD thesis, Applied mathematics, Université Marne la Vallée.

Faille, I., Thibaut, M. *et al.* 2014. Modelling fluid flow in faulted basins. *Oil & Gas Science and Technology – Rev. IFP Energies nouvelles*, **69**, 529–553, https://doi.org/10.2516/ogst/2013204

Furre, A.-K., Eiken, O., Alnes, H., Vevatne, J. and Kiaer, A. 2017. 20 years of monitoring CO_2 injection at sleipner. *Energy Procedia*, **114**, 3916–3926, https://doi.org/10.1016/j.egypro.2017.03.1523

Furre, A.-K., Warchoł, M.J., Alnes, H. and Pontén, A.S.M. 2024. Sleipner 26 years: how well-established subsurface monitoring work processes have contributed to successful offshore CO_2 injection. Geoenergy, *geoenergy2024-015*, https://doi.org/10.1144/geoenergy2024-015

Gonzalez-Penagos, F., Moretti, I., France-Lanord, C. and Guichet, X. 2015. Origins of formation waters in the Llanos foreland basin of Colombia: geochemical variation and fluid flow history. *Geofluids*, **14**, 443–458, https://doi.org/10.1111/gfl.12086

Granjeon, D. 1997. *Modélisation Stratigraphique Deterministe: Conception et Applications d'un Modèle Diffusif 3D Multilithologique*. These Doct, University of Rennes 1, France, 175.

Guichet, X., Wolf, S. and Pandi, P. 2009. Paleo-fluid flows and present hydrodynamic conditions improved by Basin modeling integrating Salinity Transport. AAPG International Conference, 15–18 November, Rio de Janeiro, Brazil, AAPG Search and Discover Article #90100.

Haddadji, R. 2006. The In-Salah CCS experience Sonatrach, Algeria. The First International Conference on the Clean Development Mechanism, 19–21 September 2006, Riyadh, Saudi Arabia.

Hantschel, T. and Wygrala, B. 2019. Petroleum systems modeling on the move: scientific concepts, numerical models and exploration practices. AAPG Hedberg Conference, The Evolution of Petroleum Systems Analysis: Changing of the Guard from Late Mature Experts to Peak Generating Staff, 4–6 March 2019, Houston, Texas. AAPG Datapages/Search and Discovery Article #90349.

Kauerauf, A. and Hantschel, T. 2009. *Fundamentals of Basin and Petroleum Systems Modeling*. Springer Berlin, Heidelberg, 476, https://doi.org/10.1007/978-3-540-72318-9

Lemgruber, A., Gonçalves, F., Loures, L., Palmowski, D., Rostirolla, S., Zagotto, E. and Araujo, A. 2010. The use of seismic inversion results as an input in a high-resolution petroleum system modelling in the Santos basin, Brazil. Adapted from oral presentation at AAPG Annual Convention and Exhibition, 11–14 April 2010, New Orleans, Louisiana. Search and Discovery Article #40585.

Li, W.-C., Borgese, C., Benedicto, A., Ray, N. and Sokolov, D. 2021. Singular structured hexahedral grid. RING Meeting 2021, Vandoeuvre-lès-Nancy, France. hal-03375671.

Medellin, F., Fehler, L., Louni, N. and Laigle, J.M. 2018. Pore pressure prediction from basin simulation of heat and fluid flow: application to a realistic earth model in the Gulf of Mexico. Adapted from an Extendend Abstract Based on Oral Presentation Given at 2018 AAPG Annual Convention & Exhibithion, 20–23 May 2018, Salt Lake City, Utah. Search and Discovery Article #42287.

Mello, U. and Karner, G. 1996. Development of sediment overpressure and its effect on thermal maturation: application to the Gulf of Mexico basin. *AAPG Bulletin*, **80**, 1367–1396, https://doi.org/10.1306/64ED9A42-1724-11D7-8645000102C1865D

Michael, K., Golab, A., Shulakova, V., Ennis-King, J., Allinson, G., Sharma, S. and Aiken, T. 2010. Geological storage of CO_2 in saline aquifers – a review of the experience from existing storage operations. *International Journal of Greenhouse Gas Control*, **4**, 659–667, https://doi.org/10.1016/j.ijggc.2009.12.011

Perrier, R. and Quiblier, J. 1974. Thickness changes in sedimentary layers during compaction history; methods for quantitative evolution. *AAPG Bulletin*, **58**, 507–520.

Ringrose, P., Andrews, J., Zweigel, P., Furre, A.K., Hern, B. and Nazarian, B. 2022. Why CCS is not like reverse gas engineering. *First Break*, **40**, 85–91, https://doi.org/10.3997/1365-2397.fb2022088

Schneider, F., Burrus, J. and Wolf, S. 1993. Modelling overpressures by effective-stress /porosity relationships in low-permeability rocks: empirical artifice or physical reality? *In:* Doré, A.G., Augustson, J.H., *et al.* (eds) *Basin Modelling: Advances and Applications*. *NPF Special Publications*, **3**. Elsevier, Amsterdam, 333–341.

Schneider, F., Bouteca, M. and Sarda, J. 1999. Hydraulic fracturing at sedimentary basin scale. *Oil & Gas Science and Technology*, **54**, 797–806, https://doi.org/10.2516/ogst:1999067

Schneider, F., Nadeau, P. and Hay, S. 2003. Model of shale permeability as a function of the temperature – application to Mesozoic mudstones, Egersund basin, Norwegian continental shelf. EAGE 65th Conference and Exhibition, 2–5 June 2003, Stavanger, Norway.

Schneider, F., Rousse, S., Faure, J., Lemgruber, A., Gutierrez, G., Pareja, J. and Padilla, O. 2020. Hydrocarbons potential of the eastern Madre de Dios basin, Bolivia. *In:* Zamora, G., McClay, K.R. and Ramos, V.A. (eds) *Petroleum Basins and Hydrocarbon Potential of the Andes of Peru and Bolivia*. *AAPG Memoir*, **117**, 413–442.

Steckler, M.S. and Watts, A.B. 1978. Subsidence of the Atlantic-type continental margin off New York. *Earth and Planetary Science Letters*, **41**, 1–13, https://doi.org/10.1016/0012-821X(78)90036-5

Steckler, M., Berthelot, F., Lyberis, N. and Le Pichon, X. 1988. Subsidence in the gulf of suez: implications for rifting and plate kinematics. *Tectonophysics*, **153**, 249–270, https://doi.org/10.1016/0040-1951(88)90019-4

Torelli, M., Kowalewski, I. *et al.* 2021. Quantification of natural microbial methane from generation to emission in the offshore Aquitaine: a basin modelling approach. *Marine and Petroleum Geology*, **127**, 104949, https://doi.org/10.1016/j.marpetgeo.2021.104949

Ungerer, P., Burrus, J., Doligez, B., Chenet, P.Y. and Bessis, F. 1990. Basin evaluation by integrated two-dimensional modelling of heat transfer, fluid flow, hydrocarbon genetation and, migration. *AAPG Bulletin*, **74**, 309–335, https://doi.org/10.1306/0C9B22DB-1710-11D7-8645000102C1865D

Woillez, M.L., Souque, C., Rudkiewicz, J.L., Willien, F. and Cornu, T. 2017. Insights in fault flow behaviour from onshore Nigeria petroleum system modelling. *Oil & Gas Science and Technology – Rev. IFP Energies nouvelles*, **72**, 31, https://doi.org/10.2516/ogst/2017029